Optical properties of scandium-doped aluminum nitride thin film for integrated photonics

Nanxi Li[a]*, Yangyang Zhuge[a,b], Wing Wai Chung[a], Xiangxin Gong[a,c], Siyu Xu[a,b], Yanmei Cao[a], Minghua Li[a], Yat Fung Tsang[a], Yeow Teck Toh[a], Steven Hou Jang Lee[a], Huamao Lin[a], Landobasa Y M Tobing[a,d], Chong Pei Ho[a], Sang Hoon Chae[c,e], Xianshu Luo[a,d], and Chengkuo Lee[b#]

[a]Institute of Microelectronics (IME), Agency for Science, Technology and Research (A*STAR), 2 Fusionopolis Way, Innovis #08-02, Singapore 138634, Republic of Singapore
[b]Center for Intelligent Sensors and MEMS, Department of Electrical and Computer Engineering, National University of Singapore, 4 Engineering Drive 3, Singapore, 117583
[c]School of Electrical and Electronic Engineering, Nanyang Technological University, 50 Nanyang Ave, Singapore, 639798
[d]National Semiconductor Translation and Innovation Centre (NSTIC), 1 Fusionopolis Way, #19-10 Connexis North, Singapore, 138632
[e]School of Materials Science and Engineering, Nanyang Technological University, 50 Nanyang Ave, Singapore, 639798

ABSTRACT

Scandium (Sc)-doped aluminum nitride (AlN) has been widely used as a piezoelectric material in micro-electromechanical systems (MEMS) devices. Recently, it also draws interests in photonics research contributed by its enhanced nonlinear optical property. Here, we report the (n, k) values of Sc-doped AlN thin films under various doping concentrations. These thin films with thickness of around 500 nm are deposited on silica through co-sputtering process. Reduced optical bandgap energies are observed at higher Sc doping concentrations. Furthermore, the top surface roughness of < 1 nm has been obtained through atomic force microscopy (AFM) measurement for the 30% Sc-doped AlN film in a 1 × 1 μm^2 region. Also, with etching process optimization, the 10% Sc-doped photonic waveguide sidewall angle and roughness have been obtained as >80° and < 5 nm, respectively. Additionally, the patterned microring cavity has been characterized, with estimated intrinsic Q of 5.54×10^4. The reported results here pave the way towards Sc-doped AlN for integrated photonics, with potential applications in communication, sensing, and quantum computing.

Keywords: Integrated optics devices; Integrated optics materials.

1. INTRODUCTION

Scandium (Sc)-doped aluminum nitride (AlN) and AlN have been widely used as a piezoelectric material in micro-electromechanical systems (MEMS) devices for various applications [1–9]. AlN is a wide bandgap material with significant second order and third order nonlinear optical properties, and hence has been widely studied as a photonic material, with various functional devices demonstrated at different wavelength regimes [10–19]. Recently, Sc-doped AlN also draws interests from photonics research community contributed by its enhanced nonlinear optical property comparing with pure AlN. Photonic integrated circuits (PIC) based on Sc-doped AlN, including passive waveguide and microring resonator, have been demonstrated [20–24]. Furthermore, active devices including phase shifter and modulator based on nonlinear optical effect (Pockels effect) of Sc-doped AlN have also been recently reported [25–27].

In this work, we report the (n, k) values of Sc-doped AlN thin films under various doping concentrations. These thin films with thickness of around 500 nm are deposited on silica through co-sputtering process, which is complementary metal-oxide semiconductor (CMOS)-compatible and can be used for 8-inch or 12-inch wafer-scale fabrication process.

*linx1@ime.a-star.edu.sg; phone 65 6770 5485; www.a-star.edu.sg

#elelc@nus.edu.sg; phone 65 6516 5865; www.nus.edu.sg

Furthermore, the optical bandgap energies of these thin films have been estimated from Spectroscopic Ellipsometry measurement data, with reduced optical bandgap observed for higher doping concentrations. For Sc doping concentrations of 0%, 10%, 20% and 30%, the estimated optical bandgap energies are 5.7 eV, 5.4 eV, 5.0 eV, and 4.7 eV, respectively. Also, the top surface roughness of < 1 nm has been obtained through atomic force microscopy (AFM) measurement for the 500 nm thick 30% Sc-doped AlN film deposited on thermal oxide in a 1×1 μm^2 region. Additionally, with etching process optimization, the 10% Sc-doped AlN photonic waveguides have been patterned on wafer scale through CMOS-compatible fabrication process, with sidewall angle and roughness obtained as > 80° and <5 nm, respectively. Lastly, the patterned 10% Sc-doped AlN microring resonator has been characterized, with extracted loaded Q of 2.27×10^4 reported, which corresponds to an estimated intrinsic Q of 5.54×10^4. Further characterizations on wafer-scale with device design variation can be conducted. The reported results here pave the way towards low-loss Sc-doped AlN for PIC, with potential applications in optical communication, optical interconnects, sensing, and quantum computing.

2. SCANDIUM-DOPED ALUMINUM NITRIDE THIN FILM PREPARATION AND CHARACTERIZATION

The Sc-doped AlN thin films are prepared at the Institute of Microelectronics (IME) using physical vapor deposition (PVD) process. Different from our earlier reports [22,24], in this work, the Sc-doped AlN thin films are deposited through a reactive co-sputtering process, with Al and Sc as separate targets within the deposition chamber (tool model: Evatec Clusterline(R) 200E; deposition chamber: MultiSource Quattro). Compared with the PVD process using the target with fixed Sc doping concentration, the co-sputtering process has the advantage of ease control on Sc doping level. Such flexibility in doping concentration is expected especially when various doping concentrations or high doping level is required [25].

2.1 Refractive index and energy bandgap from Spectroscopic Ellipsometry

By varying the electrical power applied on Sc target, Sc-doped AlN thin films with various doping levels (0%, 10%, 20%, and 30%) have been prepared on silica substrate. The cross-sectional scanning electron microscopy (SEM) image of the deposited 30% Sc-doped AlN thin film is presented in Fig. 1(a), which indicates smooth top surface and well-controlled thickness from PVD.

The (n, k) value of these thin films have been obtained from Spectroscopic Ellipsometry, as shown in Fig. 1(b) and 1(c), respectively. From Fig. 1(b), it can be observed that the refractive index (n) increases for higher doping concentration at the wavelength range of >200 nm. Also, the corresponding extinction coefficient (k) has the increasing trend at higher doping level, as shown in Fig. 1(c). Such trend indicates that, at a fixed wavelength, more electrons will transit from valence band to conduction band within AlN with higher Sc doping, and hence, contributes to higher optical loss in Sc-doped AlN thin film. In addition, for each Sc doping concentration, the fitting results of n and k values are self-consistent, which satisfy the Kramers–Kronig relation.

Fig. 1(d) shows the plot of fitted transmission intensity with respect to the photon energy from the Spectroscopic Ellipsometry measurement, where the optical bandgap energy can be estimated as the transmission intensity approaches 0. The estimated optical bandgap energies for Sc doping concentrations of 0%, 10%, 20% and 30% is 5.7 eV, 5.4 eV, 5.0 eV, and 4.7 eV, respectively. These are the lowest energies where photons begin to be absorbed in Sc-doped AlN thin film. Alternatively, the optical bandgap energy of the Sc-doped AlN material can also be obtained via the method of Jan Tauc [28–30], which is done through Tauc plot of the relation among absorption coefficient, photon energy, and material optical bandgap energy. The absorption coefficient of the material can be calculated from the extinction coefficient (k) value. The optical bandgap energies of our Sc-doped AlN thin films obtained from Tauc plot are slightly higher but comparable with the estimated values above.

Additionally, the reduced bandgap energies at higher doping level also indicates that electrons are easier to transit from valence band to conduction band and hence creates absorption. Meanwhile, at higher doping level, Sc-doped AlN thin film has potentially higher electro-optical (EO) coefficient [25]. Therefore, there is a trade-off between EO modulation efficiency and waveguide loss.

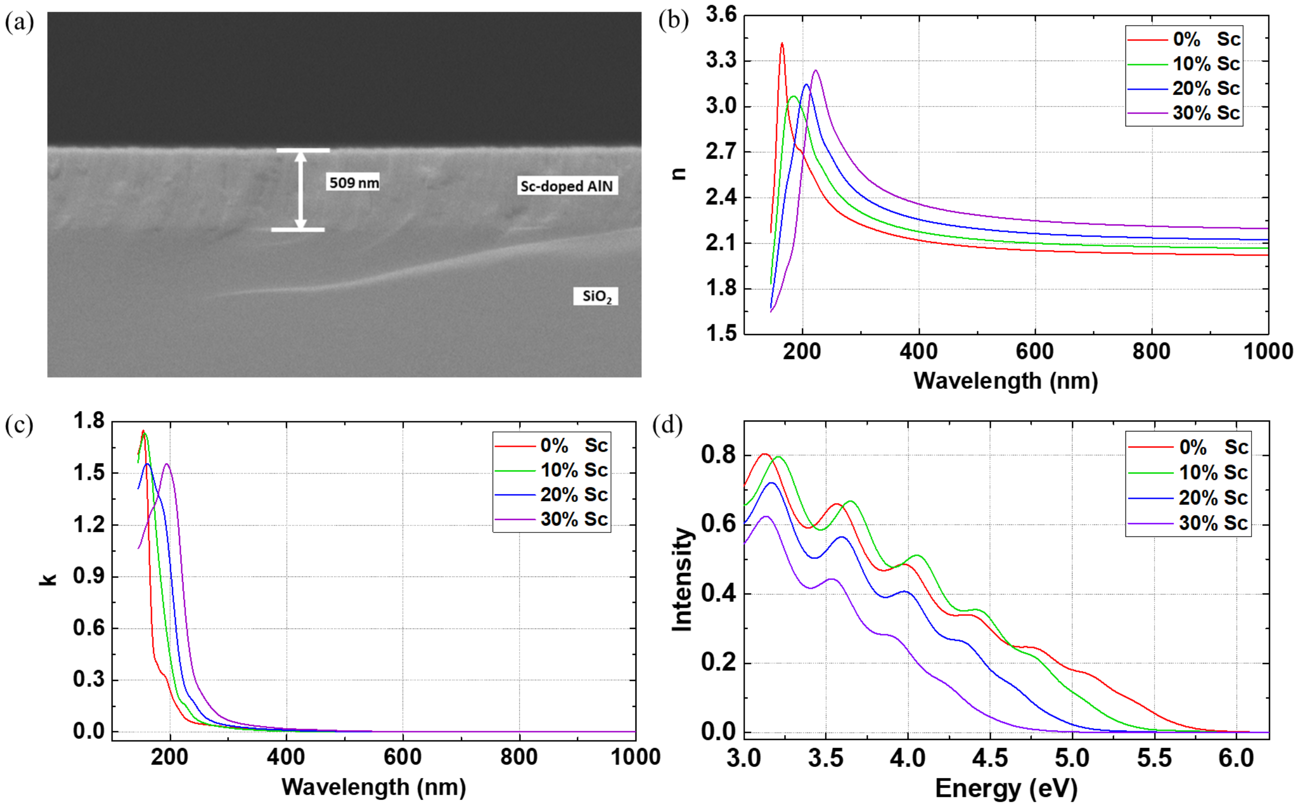

Figure 1. (a) Cross sectional SEM image of 30% Sc-doped AlN thin film on silica substrate. (b) Refractive index (n) of Sc-doped AlN under various doping concentrations. (c) Extinction coefficient (k) of Sc-doped AlN under various doping concentrations. (d) Fitted transmission intensity with respect to photon energy in eV.

2.2 Thin film top surface roughness from Atomic Force Microscopy

Thin films with smooth top surface roughness are preferred for PIC as it contributes to low scattering loss in photonic waveguide. By using the same deposition tool and process, Sc-doped AlN with various doping concentrations have also been deposited on thermal oxide on top of 8-inch Si wafer substrate, which can be further processed to form photonic waveguides. Its top surface roughness has been measured through Atomic Force Microscopy (AFM). Fig. 2(a) and 2(b) shows the AFM measurement results from 30% Sc-doped AlN thin film. From these images, the crystal grains can be clearly observed, which indicates the poly-crystalline structure of the thin film. With scanning area of 1×1 μm^2, the surface roughness of the sample has been obtained as low as 0.96 nm. Such roughness should be contributed by the columnar structure of the lattice.

An additional note worth mentioning is that comparing with another commonly used photonic material, silicon nitride (Si_3N_4) thin film grown by low pressure chemical vapor deposition (LPCVD), the top surface roughness of our Sc-doped AlN thin film is still relatively higher, but within the same level of magnitude. Chemical-mechanical planarization (CMP) process can be applied to further reduce the top surface roughness of Sc-doped AlN thin film.

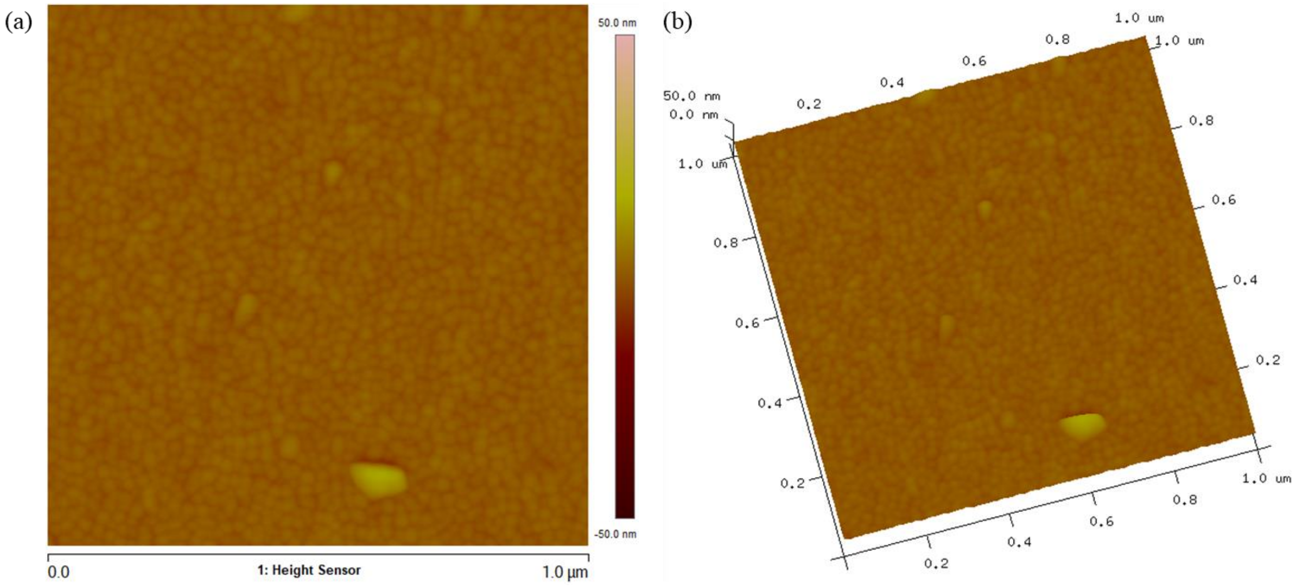

Figure 2. (a) 2D and (b) 3D AFM measurement results of 30% Sc-doped AlN deposited on thermal oxide on top of Si substrate, with surface roughness value of 0.96 nm.

2.3 Photonic waveguide sidewall angle and roughness

In PIC, waveguide with vertical sidewall angle and smooth sidewall roughness are also preferred as it brings high optical mode confinement, well critical dimension (CD) control, and low optical loss. On top of our developed Sc-doped AlN waveguide etching process on 8-inch wafer [24], we have optimized the etching recipe to achieve vertical sidewall angle. The 10% Sc-doped AlN waveguide with sidewall angle of > 80° and waveguide width of 1 µm is presented in Fig. 3(a). Such sidewall angle is higher than the ones from earlier reported Sc-doped AlN waveguides, which are typically around 70° [20–22,24]. The etched Sc-doped AlN waveguide with remaining SiO_2 hardmask (HM) on top is also included in Fig. 3(b). From the 3D AFM measurement, the side-wall roughness is found to be < 5 nm. Such developed patterning process can be used for functional photonic devices based on Sc-doped AlN PIC. In addition, for Sc-doped AlN with higher doping concentration (20%, or even 30%), we found the material becomes harder to etch by using the same etching recipe. The etching recipe needs to be adjusted for different Sc doping concentration.

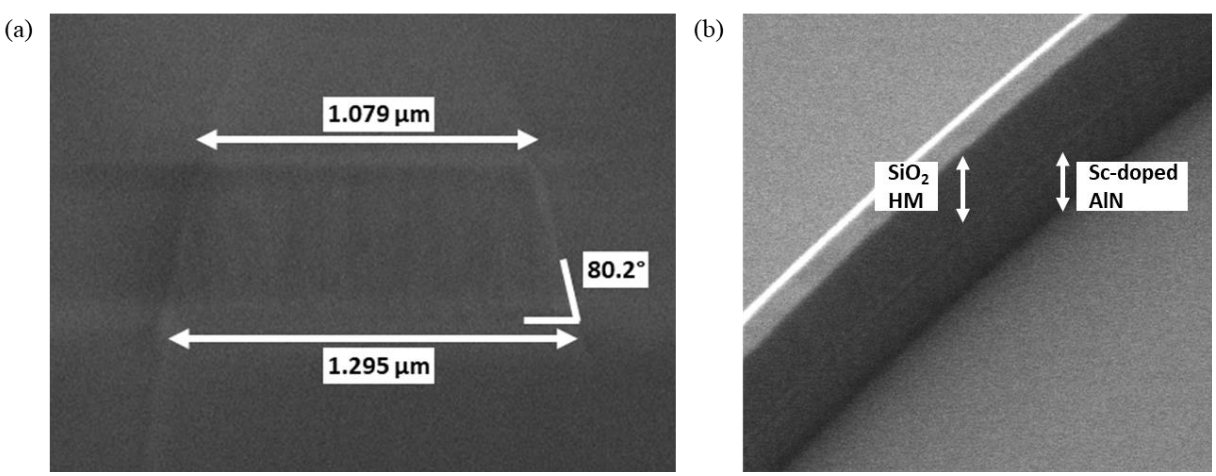

Figure 3. (a) Cross sectional SEM image of 10% Sc-doped AlN with side-wall angle of > 80°. (b) Etched 10% Sc-doped AlN waveguide with remaining SiO_2 hardmask (HM) on top.

2.4 Microring resonator cavity and Q value

After patterning of 10% Sc-doped AlN waveguide on 8-inch wafer scale, top oxide cladding was deposited to form the photonic waveguide structure, followed by deep trench etching process for edge coupling through optical fiber, and finally an annealing process to reduce the material loss. The microring resonator characterization results are presented in Fig. 4. The Sc-doped AlN microring has a radius of 160 µm. Both microring and bus waveguide have a designed width of 1 µm, and the coupling gap between them are designed to be 0.8 µm. A tunable laser is synchronized with a photodetector for wavelength sweeping, with setup schematic shown in Fig. 4(a). The passive response of the microring in dB scale is presented in Fig. 4(b). With Lorentzian fitting on one of the resonances in linear scale as shown in Fig. 4(c), the loaded Q of the microring can be extracted to be 2.27×10^4, and the corresponding intrinsic Q can be estimated to be 5.54×10^4 (assuming critical coupling). Further wafer-scale characterizations on photonic devices with design variations can be conducted.

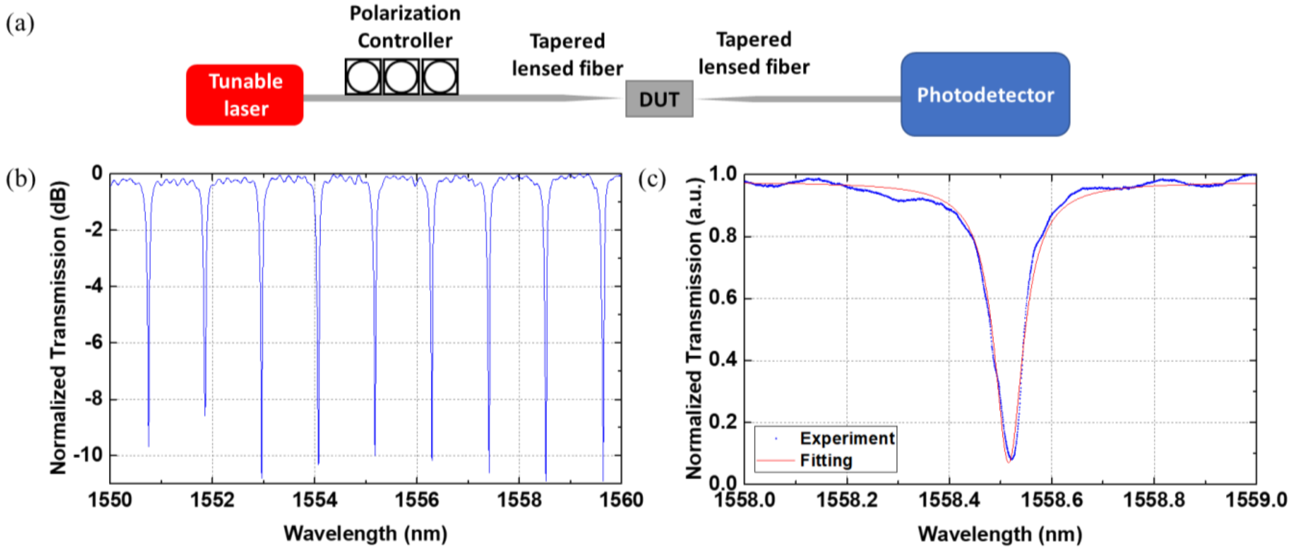

Figure 4. (a) Schematic of characterization setup for microring resonator photonic device. DUT: device under test. (b) Passive response of microring resonator in log scale at C-band. (c) Resonance spectrum of microring cavity in linear scale, indicating loaded Q of 2.27×10^4, and the corresponding estimated intrinsic Q of 5.54×10^4.

3. CONCLUSION

To sum up, the (n, k) values of Sc-doped AlN thin films under various doping concentrations have been reported. These thin films with thickness of around 500 nm are deposited on silica through co-sputtering process. Also, reduced bandgap has been observed for higher doping concentrations: based on Spectroscopic Ellipsometry measurement data, for Sc doping concentrations of 0%, 10%, 20% and 30%, the optical bandgap energies are estimated to be 5.7 eV, 5.4 eV, 5.0 eV, and 4.7 eV, respectively. Furthermore, the top surface roughness of < 1 nm has been obtained through AFM for the 500 nm thick 30% Sc-doped AlN film deposited on thermal oxide in a 1 × 1 µm^2 region. Also, with etching process optimization, the 10% Sc-doped photonic waveguides have been patterned on wafer scale, with sidewall angle and roughness obtained as > 80° and < 5 nm, respectively. Additionally, the pattern of 10% Sc-doped AlN microring resonator has been characterized, with loaded Q of 2.27×10^4 obtained, which corresponds to an estimated intrinsic Q of 5.54×10^4. Future work includes wafer-level device characterization with design variations. The reported results pave the way towards low-loss Sc-doped AlN for PIC for various applications in optical communication, optical interconnect, sensing, and quantum computing.

ACKNOWLEDGEMENTS

This work is supported by Agency for Science, Technology and Research (A*STAR) under grant no. M23M5a0069 for fabrication, grant no. C220415015 for characterization and grant no. M23M6c0109 for results analysis. The authors appreciate Nina Hong for assistance on ellipsometry measurement and discussion, Yunjie Chen for assistance on AFM measurement, and Wenwei Zhou for assistance on device fabrication and characterization. Sang Hoon Chae acknowledges the support from the Singapore Ministry of Education (MOE) Academic Research Fund (AcRF) Tier 1 grants (RT2/23).

REFERENCES

[1] Sinha, N., Wabiszewski, G. E., Mahameed, R., Felmetsger, V. V., Tanner, S. M., Carpick, R. W. and Piazza, G., "Piezoelectric aluminum nitride nanoelectromechanical actuators," Appl. Phys. Lett. **95**(5), 053106 (2009).

[2] Karabalin, R. B., Matheny, M. H., Feng, X. L., Defaÿ, E., Le Rhun, G., Marcoux, C., Hentz, S., Andreucci, P. and Roukes, M. L., "Piezoelectric nanoelectromechanical resonators based on aluminum nitride thin films," Appl. Phys. Lett. **95**(10), 103111 (2009).

[3] Xu, L., Ng, D. K. T., Chen, W., Li, N., Ho, C. P., Goh, D. J., Zhang, Y., Zhang, Q. and Lee, L. Y. T., "Low-power contactless button system based on MEMS ScAlN pyroelectric detector," MOEMS and Miniaturized Systems XXII **12434**, 18–23, SPIE (2023).

[4] Wu, G., Zhu, Y., Merugu, S., Wang, N., Sun, C. and Gu, Y., "GHz spurious mode free AlN lamb wave resonator with high figure of merit using one dimensional phononic crystal tethers," Appl. Phys. Lett. **109**(1), 013506 (2016).

[5] Fei, C., Liu, X., Zhu, B., Li, D., Yang, X., Yang, Y. and Zhou, Q., "AlN piezoelectric thin films for energy harvesting and acoustic devices," Nano Energy **51**, 146–161 (2018).

[6] Li, N., Fong, A. W. K., Wang, H., Lim, L. W., Tobing, L. Y. M., Chua, Y. D., Xu, L., Chen, W., Zhang, Q., Cai, H., Wang, Q. J. and Lee, L. Y. T., "An integrated MEMS thermal emitter with piezoelectric actuation," MOEMS and Miniaturized Systems XXII **12434**, 142–146, SPIE (2023).

[7] Q. Wang, Y. Lu, S. Mishin, Y. Oshmyansky, and D. A. Horsley., "Design, Fabrication, and Characterization of Scandium Aluminum Nitride-Based Piezoelectric Micromachined Ultrasonic Transducers," Journal of Microelectromechanical Systems **26**(5), 1132–1139 (2017).

[8] Cai, H., Khairy, M. H., Ang, R. C. F., Xu, L., Ng, D. K. T., Li, N., Gu, Z., Kong, A., Chen, W., Seit, W. W., Ching, E. W. L., Jaafar, N., Wang, H., Tobing, L. Y. M., Lim, L. W., Zhang, Q. and Lee, L. Y. T., "On-chip CO2 sensor integrated with MEMS emitter and pyroelectric detector," Silicon Photonics XVIII **12426**, 103–107, SPIE (2023).

[9] Schneider, M., DeMiguel-Ramos, M., Flewitt, A. J., Iborra, E. and Schmid, U., "Scandium Aluminium Nitride-Based Film Bulk Acoustic Resonators," Proceedings **1**(4) (2017).

[10] Li, N., Ho, C. P., Zhu, S., Fu, Y. H., Zhu, Y. and Lee, L. Y. T., "Aluminium nitride integrated photonics: a review," Nanophotonics **10**(9), 2347–2387 (2021).

[11] Xiong, C., Pernice, W. H. P. and Tang, H. X., "Low-Loss, Silicon Integrated, Aluminum Nitride Photonic Circuits and Their Use for Electro-Optic Signal Processing," Nano Lett. **12**(7), 3562–3568 (2012).

[12] Lin, P. T., Jung, H., Kimerling, L. C., Agarwal, A. and Tang, H. X., "Low-loss aluminium nitride thin film for mid-infrared microphotonics," Laser Photonics Rev. **8**(2), L23–L28 (2014).

[13] Li, N., Ho, C. P., Cao, Y., Zhu, S., Chen, G. F. R., Fu, Y. H., Zhu, Y., Tan, D. T. H. and Lee, L. Y. T., "Aluminum Nitride Photonics Platforms on Silicon Substrate," Conference on Lasers and Electro-Optics (2021), paper STh2H.3, Optical Society of America (2021).

[14] Bruch, A. W., Liu, X., Gong, Z., Surya, J. B., Li, M., Zou, C.-L. and Tang, H. X., "Pockels soliton microcomb," Nat. Photon. **15**(1), 21–27 (2021).

[15] Liu, X., Bruch, A. W., Gong, Z., Lu, J., Surya, J. B., Zhang, L., Wang, J., Yan, J. and Tang, H. X., "Ultra-high-Q UV microring resonators based on a single-crystalline AlN platform," Optica **5**(10), 1279–1282 (2018).

[16] Li, N., Tobing, L. Y. M., Zhu, S. and Xue, J., "High-Q Microdisk Resonator on Aluminum Nitride Photonics Platform," CLEO 2024, paper JTh2A.28, Optica Publishing Group (2024).

[17] Majkić, A., Puc, U., Franke, A., Kirste, R., Collazo, R., Sitar, Z. and Zgonik, M., "Optical properties of aluminum nitride single crystals in the THz region," Opt. Mater. Express **5**(10), 2106–2111 (2015).

[18] Growden, T. A., Zhang, W., Brown, E. R., Storm, D. F., Meyer, D. J. and Berger, P. R., "Near-UV electroluminescence in unipolar-doped, bipolar-tunneling GaN/AlN heterostructures," Light Sci. Appl. **7**(2), 17150–17150 (2018).

[19] Li, N., Lim, L. W., Xue, J., Ho, C. P., Zhu, S., Fu, Y. H. and Lee, L. Y. T., "Aluminum Nitride Nanophotonic Phased Array on an 8-inch Silicon Wafer," CLEO 2023 (2023), paper AM3M.5, AM3M.5, Optica Publishing Group (2023).

[20] Xiong, Z., Zhang, X., Li, Z., Liu, X., Qiu, Y., Zhao, X., Zheng, S., Zhong, Q., Dong, Y. and Hu, T., "Aluminum scandium nitride on 8-inch Si wafers: material characterization and photonic device demonstration," Opt. Express, **32**(10), 17525–17534 (2024).

[21] Zhu, S., Zhong, Q., Li, N., Hu, T., Dong, Y., Xu, Z., Zhou, Y., Fu, Y. H. and Singh, N., "Integrated ScAlN Photonic Circuits on Silicon Substrate," Conference on Lasers and Electro-Optics, STu3P.5, Optical Society of America, Washington, DC (2020).

[22] Wang, S., Dhyani, V., Mohanraj, S. S., Shi, X., Varghese, B., Chung, W. W., Huang, D., Lim, Z. S., Zeng, Q., Liu, H., Luo, X., Leong, V., Li, N. and Zhu, D., "CMOS-compatible photonic integrated circuits on thin-film ScAlN," APL Photonics **9**(6), 066109 (2024).

[23] Friedman, B., Barth, S., Schreiber, T., Bartzsch, H., Bain, J. and Piazza, G., "Measured optical losses of Sc doped AlN waveguides," Opt. Express **32**(4), 5252–5260 (2024).

[24] Li, N., Chung, W. W., Goh, J. S., Tsang, Y. F., Tobing, L. Y. M., Ho, C. P., Varghese, B., Lim, L. W., Li, M., Lin, H., Zhang, Q., Ng, D. K. T., Lee, L. Y. T. and Luo, X., "Scandium-doped aluminum nitride photonic integration platform," Integrated Optics: Devices, Materials, and Technologies XXVIII **12889**, 63–66, SPIE (2024).

[25] Yang, G., Wang, H., Mu, S., Xie, H., Wang, T., He, C., Shen, M., Liu, M., Van de Walle, C. G. and Tang, H. X., "Unveiling the Pockels coefficient of ferroelectric nitride ScAlN," Nat Commun **15**(1), 9538 (2024).

[26] Yoshioka, V., Jin, J., Zhou, H., Tang, Z., Iii, R. H. O. and Zhen, B., "CMOS-compatible, AlScN-based integrated electro-optic phase shifter," Nanophotonics **13**(18), 3327–3335 (2024).

[27] Xu, T., Liu, Y., Pu, Y., Yang, Y., Zhong, Q., Zhao, X., Qiu, Y., Dong, Y., Wu, T., Zheng, S. and Hu, T., "Silicon-integrated scandium-doped aluminum nitride electro-optic modulator," arXiv:2405.18717 (2024).

[28] Tauc, J., Grigorovici, R. and Vancu, A., "Optical Properties and Electronic Structure of Amorphous Germanium," physica status solidi (b) **15**(2), 627–637 (1966).

[29] Tauc, J., "Optical properties and electronic structure of amorphous Ge and Si," Materials Research Bulletin **3**(1), 37–46 (1968).

[30] Makuła, P., Pacia, M. and Macyk, W., "How To Correctly Determine the Band Gap Energy of Modified Semiconductor Photocatalysts Based on UV–Vis Spectra," J. Phys. Chem. Lett. **9**(23), 6814–6817 (2018).